

## HOMDYN Study for the LCLS RF Photo-Injector

M. Ferrario<sup>#</sup>, J. E. Clendenin<sup>\*</sup>, D. T. Palmer<sup>\*</sup>, J. B. Rosenzweig<sup>^</sup>, L. Serafini<sup>+</sup>

<sup>#</sup> *INFN - Laboratori Nazionali di Frascati,  
Via E. Fermi 40, 00044 Frascati (Roma), Italy*

<sup>\*</sup> *Stanford Linear Accelerator Center  
Stanford University, Stanford, CA 94309*

<sup>^</sup> *UCLA, Dept. of Physics and Astronomy, Los Angeles, CA 90095*

<sup>+</sup> *INFN - Sezione di Milano, Via Celoria 16, 20133 Milano, Italy*

Contributed to 2nd ICFA Advanced Accelerator Workshop on The Physics of High  
Brightness Beams, 11/9/1999—11/12/1999, Los Angeles, CA, USA

---

*Stanford Linear Accelerator Center, Stanford University, Stanford, CA 94309*

Work supported by Department of Energy contract DE-AC03-76SF00515.

# HOMDYN STUDY FOR THE LCLS RF PHOTO-INJECTOR

M. FERRARIO

*Istituto Nazionale di Fisica Nucleare  
Laboratori Nazionali di Frascati  
00044 Frascati (Roma), Italy*

J. E. CLENDENIN AND D. T. PALMER

*Stanford Linear Accelerator Center  
Stanford University, Stanford, CA 94309*

J. B. ROSENZWEIG

*University of California Los Angeles  
Department of Physics and Astronomy  
Los Angeles, CA 90095*

L. SERAFINI

*Istituto Nazionale di Fisica Nucleare  
Sezione di Milano  
Via Celoria 16, 20133 Milano, Italy*

We report the results of a recent beam dynamics study, motivated by the need to redesign the LCLS photoinjector, that led to the discovery of a new effective working point for a split RF photoinjector. The HOMDYN code, the main simulation tool adopted in this work, is described together with its recent improvements. The new working point and its LCLS application is discussed. Validation tests of the HOMDYN model and low emittance predictions, 0.3 mm-mrad for a 1 nC flat top bunch, are performed with respect to the multi-particle tracking codes ITACA and PARMELA.

## 1 Introduction

The Linac Coherent Light Source (LCLS) is an X-ray Free Electron Laser (FEL) proposal that will use the final 15 GeV of the SLAC 3-km linac for the drive beam. The performance of the LCLS in the 1.5 Angstrom regime is predicated on the availability of a 1-nC, 100-A beam at the 150-MeV point with normalised rms transverse emittance of  $\sim 1$  mm-mrad. An experimental program is underway at the Gun Test Facility (GTF) at SLAC to demonstrate a high-brightness beam meeting the LCLS requirements using an rf photoinjector [1]. The design of high-brightness rf photoinjectors today is based on the development over the past decade of a rather complete theoretical understanding of how the beam properties initially evolve under the influence of the rf acceleration and a focusing solenoid field [2]. In a typical rf photoinjector design, in fact, the electron source is embedded in a high-gradient rf accelerating cavity surrounded by a solenoid to compensate for the defocusing space-charge effects. A post accelerator (booster) is then necessary to

drive the beam out of the space charge dominated regime. Post acceleration can be accomplished by additional cavities, separated from the gun by a drift (split photoinjector) or directly integrated in the gun (integrated photoinjector).

The GTF experiment uses a 1.6-cell S-band rf gun developed jointly with BNL and UCLA [3] surrounded by a solenoid just after the gun exit. After a short drift it is followed by a standard SLAC 3-m accelerating section. A transverse normalised rms emittance of 2.4 mm-mrad for a 0.9 nC pulse with 10-ps FWHM Gaussian pulse length has been measured at BNL using a similar configuration [4].

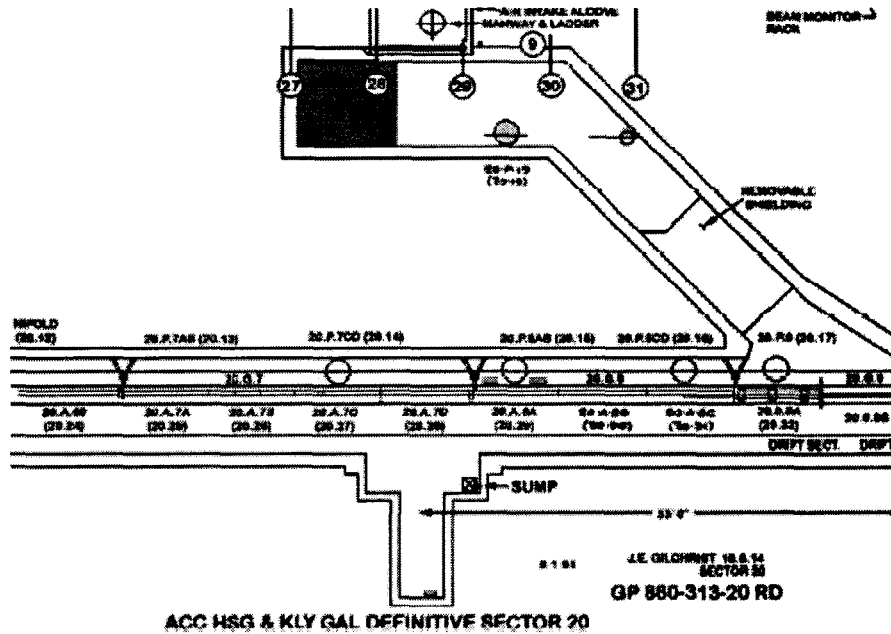


Figure 1. The off-axis empty "injector" vault, recently rediscovered at the 2/3 point of the SLAC linac, now available for the LCLS injector.

Earlier simulation studies using the multi-particle code PARMELA predicted a transverse normalised emittance of  $\sim 1$  mm-mrad - thermal emittance [5] not included - for the LCLS photoinjector if a uniform (or even a truncated Gaussian) temporal charge distribution is used [6]. While this result technically meets the LCLS requirements, it leaves no headroom for errors or practical difficulties. Consequently simulation studies have continued with the goal of finding a photoinjector design for the LCLS that would predict a transverse emittance of no more than 0.8 mm-mrad with the thermal emittance included. In addition, an off-axis empty "injector" vault, shown in Fig. 1, was recently rediscovered at the 2/3 point of the SLAC linac that is available for the LCLS injector. (The off-axis vault was first noticed in spring 1999, by the LCLS Project Engineer L. Klaisner while

inspecting 30-year old drawings of the accelerator housing.) The axial space available in this vault is only about 10 m. Since the beam must be accelerated to  $\sim 150$  MeV to eliminate any space charge effects when in the dog leg to the main linac, a new injector design that will be compatible with high-gradient acceleration has become highly desirable.

During the redesign work, as will be reported in this paper, a new effective working point for a split RF photoinjector has been discovered. In fact by a proper choice of RF gun and solenoid parameters, the emittance evolution shows a double minimum behaviour in the drifting region [7]. If the booster is located where the relative emittance maximum and the envelope waist occur, the second emittance minimum can be shifted to the booster exit and frozen at a very low level [8], 0.3 mm-mrad for a 1 nC flat top bunch, to the extent that the invariant envelope matching conditions are satisfied [2]. Travelling wave (TW) structures embedded in a long solenoid or alternatively standing wave (SW) structures are both candidates as booster linac.

In section two of this paper we recall the main results of the invariant envelope theory and the derived matching conditions for a split photoinjector. This theory, describing the space charge dominated regime under the multi-slice envelope equations approximation, explains the rms normalised emittance oscillations as due to cold-plasma like oscillations in the beam envelope and represents an excellent tool for a first choice of the injector parameters. The code HOMDYN [9], the main simulation tool adopted in this work, is based on a similar semi-analytical model and it is described in section three together with its recent enhancements. Validation tests of the HOMDYN model are discussed in section four with respect to a multi-particle tracking code: ITACA. In section five we discuss the new working point for a split photoinjector in the framework of an S-band design. The applications to the LCLS injector design are described in section six and an inspection of non-linearities contribution is performed, by means of PARMELA simulations, and reported in section seven.

## 2 The theory of invariant envelope and derived matching conditions

It has been by now understood [2] that the optimisation of a photo-injector corresponds to accelerating and propagating the beam through the device as close as possible to two beam equilibrium: a laminar Brillouin flow in drifts and the so-called invariant envelope in accelerating sections, which is a generalisation of Brillouin flow for an accelerated beam. In this case the beam undergoes cold plasma oscillations, in which the space charge collective force is largely dominant over the emittance pressure. The frequency of the plasma oscillations, due to mismatches between the space charge force and the external focusing gradient, is to first order independent of the current while the betatron motion (trajectory cross-over) is almost absent (laminar flow). In fact it is the frequency independence that leads to reversible normalised emittance oscillations: accelerating the beam on the invariant envelope damps these oscillations like the square root of the beam energy, so that

the normalised emittance at the injector exit reduces to a steady state minimum when the oscillations are properly tuned.

It has been shown that the rms projected normalised emittance  $\varepsilon_n = \langle \beta\gamma \rangle \sqrt{\langle x^2 \rangle \langle x'^2 \rangle - \langle xx' \rangle^2}$  oscillates with a frequency  $\sqrt{2K_r}$  at an amplitude  $\Delta\varepsilon_n \propto \sqrt{\hat{I}/\gamma}$  whenever a bunched beam is rms matched into a focusing channel of gradient  $K_r$ , i.e. on a Brillouin flow equilibrium:

$$\sigma_B(\zeta) = \sqrt{\frac{\hat{I}(\zeta)}{2I_0\gamma^3 K_r}} \quad (1)$$

where  $\sigma$  is the rms beam spot size, eventually slice dependent,  $\zeta \equiv z - \beta ct + z_0$  is the slice position,  $\hat{I}$  is the peak current and  $I_0=17$  kA the Alfvén current. In a similar way accelerating on the invariant envelope:

$$\sigma_{inv}(\zeta) = \frac{2}{\gamma'} \sqrt{\frac{\hat{I}(\zeta)}{3I_0\gamma}} \quad (2)$$

where  $\gamma' = \frac{eE_{acc}}{m_e c^2} \approx 2E_{acc}$ ,  $E_{acc}$  is the accelerating field, which is a particular exact solution of the rms envelope equation in the laminar flow regime, leads to damped oscillations of the emittance.

The basic point in the design of a photoinjector is therefore to match properly the beam at injection into any accelerating section, according to these criteria:

$$\sigma' = 0 \quad (3)$$

implying a laminar waist at injection and

$$\gamma' = \frac{2}{\sigma_w} \sqrt{\frac{\hat{I}}{3I_0\gamma}} \quad (4)$$

or

$$\gamma' = \frac{2}{\sigma_w} \sqrt{\frac{\hat{I}}{2I_0\gamma}} \quad (5)$$

giving an rms match on the invariant envelope for a SW or TW accelerating field respectively.

The laminar regime extends up to an energy given by:

$$\gamma = \sqrt{\frac{8}{3}} \frac{\hat{I}}{2I_0\varepsilon_{th}\gamma'} \quad (6)$$

where  $\epsilon_{th}$  is the thermal emittance. With the expected LCLS parameters,  $\hat{I}=100$  A,  $E_{acc}=25$  MV/m and an estimated [5] thermal emittance of 0.3 mm-mrad for a Cu cathode with UV excitation, the transition occurs at 160 MeV. For this reason the emittance compensation process of the LCLS injector has to be optimised up to the exit of the booster linac, before injecting the beam in the main linac through the dog leg magnet system.

### 3 The HOMDYN model

Single bunch simulations of the beam dynamics performed from the photo-cathode surface up to the undulator injection at the linac exit are at the far limit of multi-particle codes like PARMELA, because CPU times of several hours are typically required. Due to the non-linearity of the problem, based on longitudinal space charge correlations within the bunch, standard rms linear space charge description as performed by matrix-based transport codes like TRACE3D are not able to describe the associated emittance. In cases where multi-bunch effects must be taken into account, because of the high repetition rate in the train and, as well, because of fluctuations in the pulse intensity and timing jitter of the laser driving the photo-cathode, a multi-particle simulation would be unaffordable. For this reason we recently enhanced the capability of the code HOMDYN, developed originally to describe multi-bunch effects in linacs, to model the beam generation at the photo-cathode in a photo-injector RF cavity. Higher mode excitation below cut-off as well as non-relativistic beam dynamics were already being modelled by the code, as reported in Ref. [9]

The basic approximation in the description of beam dynamics lies in the assumption that each bunch is described by a uniformly charged cylinder, whose length and radius can vary under a self-similar time evolution, keeping anyway uniform the charge distribution inside the bunch. By slicing the bunch in an array of cylinders (Multi-Slices Approximation), each one subject to the local field, one obtains also the energy spread and the emittance degradation due to phase correlation of RF and space charge effects.

The longitudinal space charge field on axis, inside and outside the bunch, at a distance  $\zeta_s = z_s - z_t$  of the  $s^{\text{th}}$  slice from the bunch tail located at  $z_t$ , is given by:

$$E_z^{sc}(\zeta_s) = \frac{Q}{2\pi\epsilon_0 R_s^2} H(\zeta_s, A_{r,s}) \quad (7)$$

where

$$H(\zeta_s, A_{r,s}) = \sqrt{(1 - \zeta_s/L)^2 + A_{r,s}^2} - \sqrt{(\zeta_s/L)^2 + A_{r,s}^2} - |1 - \zeta_s/L| + |\zeta_s/L| \quad (8)$$

and  $Q$  is the bunch charge,  $L$  the bunch length,  $R_s$  the slice radius and  $A_{r,s} \equiv R_s/(\gamma_s L)$  is the slice rest frame aspect ratio.

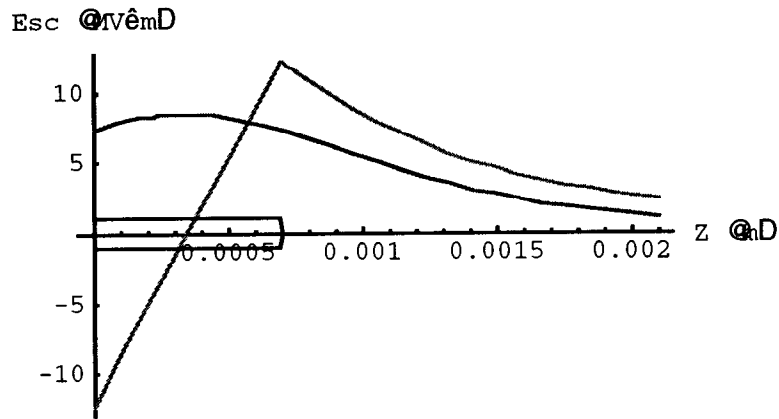


**Figure 2.** Longitudinal (red line) and Transverse (blue line) space charge field in a bunch just extracted from the cathode, image charges switched off.

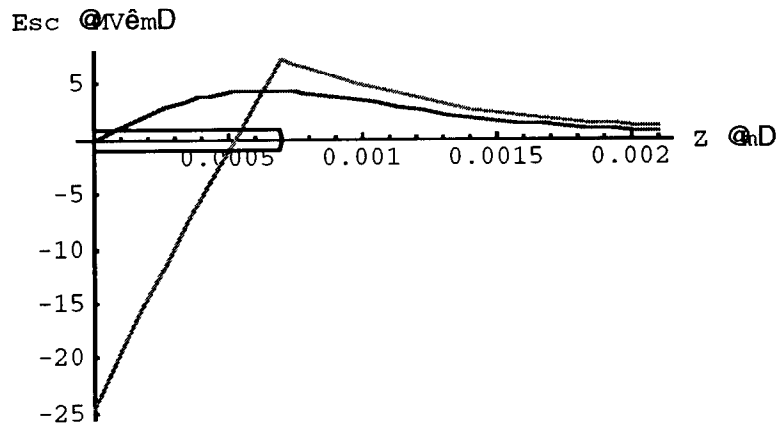


**Figure 3.** Longitudinal (red line) and Transverse (blue line) space charge field in a bunch just extracted from the cathode, image charges switched on.

The radial space charge fields on the slice envelope:

$$E_r^{sc}(\zeta_s) = \frac{Q}{4\pi\epsilon_0 R_s L} G(\zeta_s, A_{r,s}) \quad (9)$$

where

$$G(\zeta_s, A_{r,s}) = \frac{1 - \zeta_s/L}{\sqrt{(1 - \zeta_s/L)^2 + A_{r,s}^2}} + \frac{\zeta_s/L}{\sqrt{(\zeta_s/L)^2 + A_{r,s}^2}} \quad (10)$$

is obtained as a linear expansion off axis of the longitudinal component of the field (8) and represents at present the main limitation of the model. The non-linear transverse space charge contribution, in fact, may be responsible of an inner bunch charge re-distribution that may lead to emittance dilution.

The equations for the longitudinal motion for each slice are:

$$\dot{z}_s = \beta_s c \quad (11)$$

$$\dot{\beta}_s = \frac{e}{m_o c \gamma_s^3} \left( E_z^{acc}(z_s, t) + E_z^{sc}(\zeta_s, t) - E_z^{sc}(\xi_s, t) \right) \quad (12)$$

where the last term accounts for the contribution of the bunch image charges on the cathode, modeled by a counterpropagating bunch from the same origin, the cathode, with opposite charge, located at a distance  $\xi_s = z_s + z_{head}$  from the s-slice.

In Figs. 2 and 3 the on axis longitudinal space charge field (red line) and the envelope radial space charge field (blue line) are shown, for a bunch just born with the tail still on the cathode surface. In Fig. 2 image charges are switched off, while they are taken in to account in Fig. 3. The distortion of the field produced by image charges, results during the subsequent evolution in an elongation of the bunch and a lower defocusing action on the bunch tail. The bunch is shown as a black cylinder with 1 nC charge, 0.7 mm long and 1 mm radius, i. e., with an aspect ratio  $A_s = 1.4$ , resulting in a non linear radial space charge profile along the bunch.

The evolution of each slice radius  $R_s$  is described in the time-domain according to an envelope equation, including damping due to acceleration (second term), solenoid focusing (third), RF-focusing (fourth), space charge effects (fifth), image charges from the cathode surface (sixth) and thermal emittance pressure (seventh):

$$\begin{aligned} \ddot{R}_s + \beta_s \gamma_s^2 \dot{\beta}_s \dot{R}_s + (K_s^{sol} + K_s^{rf}) R_s = \\ = \frac{2c^2 k_p}{R_s \beta_s} \left( \frac{G(\zeta_s, A_r)}{\gamma_s^3} - (1 + \beta_s^2) \frac{G(\xi_s, A_r)}{\gamma_s} \right) + \left( \frac{4\epsilon_n^{th} c}{\gamma_s} \right)^2 \frac{1}{R_s^3} \end{aligned} \quad (13)$$

The dots indicate the derivation with respect to time, and

$$K_s^{sol} = \left( \frac{e B_z(z_s)}{2m_o \gamma_s} \right)^2 \quad (14)$$

is the solenoid focusing gradient. The RF focusing gradient is:

$$K_s^{rf} = \frac{e}{2\gamma_s m_o} \left( \frac{\partial E_z}{\partial z} + \frac{\beta_s}{c} \frac{\partial E_z}{\partial t} \right) \quad (15)$$



expressed through the linear expansion off-axis of the accelerating field  $E_z = E_z(0, z, t)$ . The beam perveance is:

$$k_p = \frac{I(\zeta_s)}{2I_o} \quad (16)$$

and  $\epsilon_n^{th}$  is the rms normalised thermal beam emittance.

In order to evaluate the degradation of the rms emittance produced by longitudinal correlation in space charge and transverse external forces, we use the following expression for the correlated emittance:

$$\epsilon_n^{cor} = \frac{1}{4} \sqrt{\langle R^2 \rangle \langle (\beta\gamma R')^2 \rangle - \langle R\beta\gamma R' \rangle^2} \quad (17)$$

where  $R' = \frac{d}{dz} R$  and the average  $\langle \rangle = \frac{1}{N} \sum_{s=1}^N$  is performed over the N slices.

The total rms emittance will be given by a quadratic summation of the thermal emittance and the correlated emittance:

$$\epsilon_n = \sqrt{(\epsilon_n^{th})^2 + (\epsilon_n^{cor})^2} \quad (18)$$

An effective description of the bunch generation from the cathode surface has been added to the code to properly simulate RF photoinjectors. For a given laser pulse time length  $\Lambda$  a neutral bunch ( $Q = 0$ ) of initial energy of some eV and initial length  $L_0 = \beta c \Lambda$  is generated behind the cathode location  $z_c$ , where the accelerating field is zero, with the center located at  $z_b = z_c - L_0 / 2$ . At  $t=0$  the bunch starts moving according to the equation of motion and slice by slice enters in to the RF gun cavity where each slice is activated in the envelope equation sharing an increasing bunch charge:

$$Q_{act} = Q \cdot \left( 1 - \frac{z_c - z_t}{L_0} \right) \quad (19)$$

The description of the accelerating field in a SW structure is simply obtained by a superposition of normal modes as computed by a standard electromagnetic solver like SUPERFISH [10]. When single- or multi-bunch beam loading effects [11] are negligible, only the fundamental accelerating field pattern can be taken into account. The situation is more complicated when TW structures are considered. Boundary conditions indeed require that the field in the input and output half cells of a TW structure oscillates with SW pattern [12], and in the simulations it has to be smoothly matched to the TW field pattern of the inner cells. In addition the different focusing properties of SW and TW structure [13] are very important in the beam dynamics and have to be taken correctly into account.

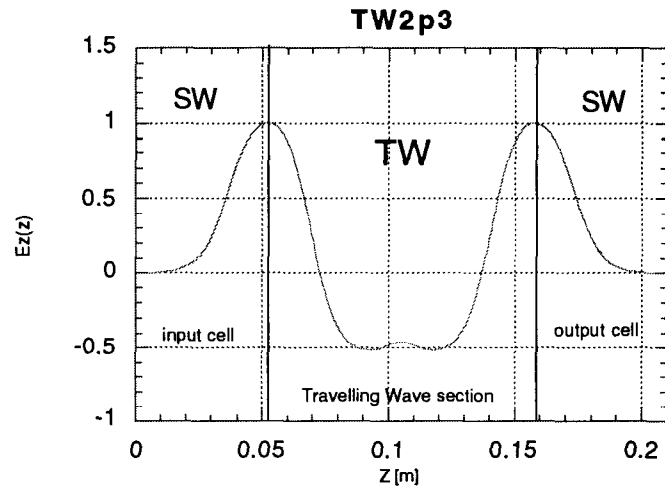


Figure 4. One period of a S-band  $2\pi/3$  mode as computed by SUPERFISH, together with the input and output half-cell patterns and their fringing fields in the beam tubes.

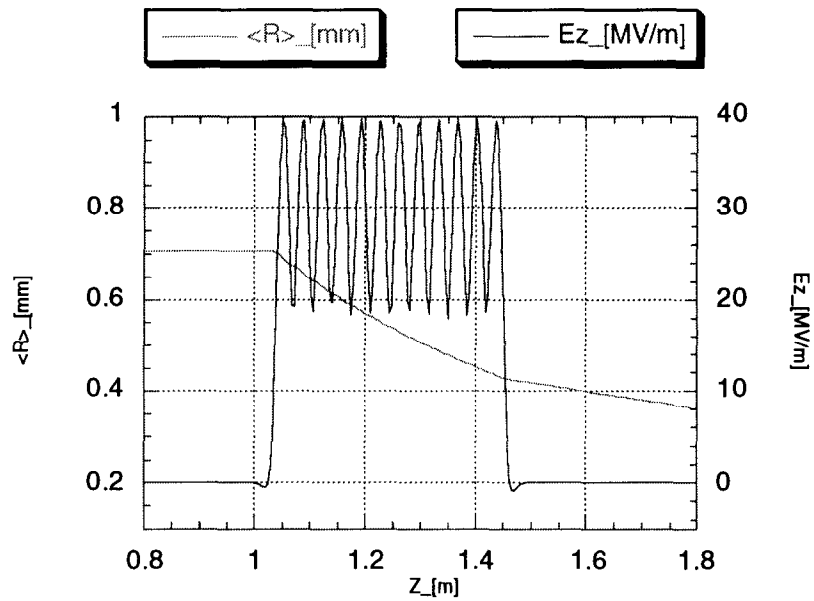


Figure 5. Accelerating field seen by the beam in a 12 cells long structure. The behaviour of the beam envelope is also shown for a relativistic low charge beam.

HOMDYN has been recently improved to include TW structures by representing the accelerating field as superposition of two standing wave patterns [14]. The on axis field for any TW mode is given simply by:

$$E_z^{TW}(z,t) = \tilde{E}_z^{SW}(z)\sin(\omega t + \phi_o + kd) - \tilde{E}_z^{SW}(z+d)\sin(\omega t + \phi_o) \quad (20)$$

with the normalisation  $\tilde{E}_z^{SW}(z) = \frac{E_z^{SW}(z)}{\sin(kd)}$ , where  $E_z^{SW}(z)$  is the corresponding SW mode pattern as computed by SUPERFISH,  $d$  is the periodicity of the structure, namely the cell length, and  $k = \frac{\omega}{c}$ .

One wave length ( $\lambda_{2\pi/3} = 3d$ ) of an S-band  $2\pi/3$  mode  $E_z^{SW}(z)$ , is shown in Fig. 4 together with the input and output half-cell patterns and their fringing field in the beam tubes. By applying eq (20) the code computes the accelerating field seen by the beam as shown, for example, in Fig. 5 for a 12 cell long structure. The behaviour of the beam envelope is also shown for a relativistic low charge beam. Clearly visible are the first order input and output kicks, generated by the SW oscillation of the extreme half cells, over the weak second order focusing effect of the pure TW field, as discussed in [13].

#### 4 The HOMDYN model validation

The validation of the HOMDYN model has been done with respect to a completely different code: ITACA [15], a multi-particle tracking code based on a self-consistent description of fields by a Cloud In Cell method [16]. From now on any emittance quoted is considered to be rms normalised with the thermal contribution set to zero.

The RF gun taken into consideration is a 1+1/2 cell gun operated at 1.3 GHz, producing a 1 nC bunch charge at 80 A peak current with the typical bunch parameters of the TTF-FEL [17] experiment. The peak RF field at the cathode is 50 MV/m with a laser spot size (hard edge) of 1.5 mm. Applying a 1.8 kG peak solenoid field, the resulting beam envelope is plotted in Fig. 6 versus the beam propagation distance  $z$ , from the cathode surface ( $z=0$ ) down through the gun (175 mm long) and the following drift section. Clearly visible is the strongly space charge dominated behaviour of the envelope going through a gentle laminar waist in the drift. The rms normalised transverse emittance is also plotted, clearly showing the emittance correction process.

The agreement between the two codes is so remarkable that it clearly proves the validity of an envelope equation based description for this specific beam physics case. Nevertheless a significant difference in the evaluation of the absolute emittance minimum is evident from the plot. A possible explanation is reported elsewhere in these proceedings [16]. We recall here the main conclusion. Cylindrical bunches with uniform charge distribution and short rise time are modelled by multi-particle codes with an outer Gaussian halo at the edge of the bunch, due to the finite size of

particles and clouds interacting with space charge fields interpolated on the mesh. The transverse space charge field will have a non-linear behaviour around the bunch edge, resulting in numerically induced emittance growth. A high-resolution radial mesh size is required to overcome this effect. In addition the maximum longitudinal mesh step size has to be of the order of the laser pulse rise time. For example, in the case of a 1 ps rise time, the mesh step size has to be lower than 100  $\mu\text{m}$ . Radial and longitudinal high-resolution results in increasing CPU time and when a flat top bunch is considered it becomes unaffordable. The finite mesh size adopted in the ITACA run (150  $\mu\text{m}$ ) could explain the disagreement shown in Fig. 6. HOMDYN is not affected by numerically induced non linear space charge fields because the self-field is computed analytically for a perfectly uniform slice, allowing also a very short CPU time. The drawback of this model as already mentioned is that the present version of HOMDYN is not yet able to describe uniform distributions with Gaussian tails and doesn't include the radial non-linear space charge field.

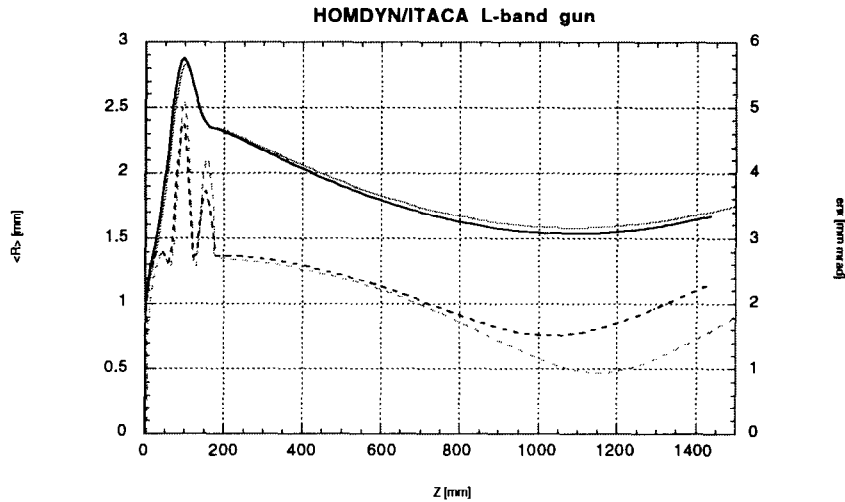


**Figure 6.** Envelope (solid lines) and emittance (dashed lines) along the TTF injector beamline as computed by HOMDYN (red lines) and ITACA (black lines).

To investigate in more details the influence of mesh size on the absolute emittance value, we recently conducted a more systematic study for a case that was under study in the framework of the FABRE [18] collaboration. We considered an integrated S-band photoinjector 10 cells long and we compared HOMDYN results with ITACA runs by changing mesh size step. The bunch input parameters were: 1nC charge, 8 ps long and 1 mm radius. The peak field on the cathode was 80 MV/m. The comparison, Fig. 7, shows an increasing agreement between the two codes about the absolute emittance minimum evaluation as long as the mesh size is reduced down to 50  $\mu\text{m}$ .

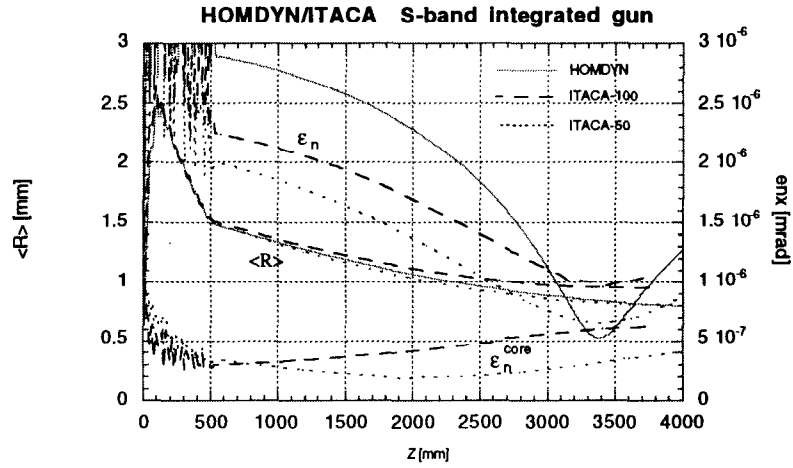


**Figure 7.** Envelope and emittance along the FABRE injector beamline as computed by HOMDYN (red lines) and ITACA (black lines).

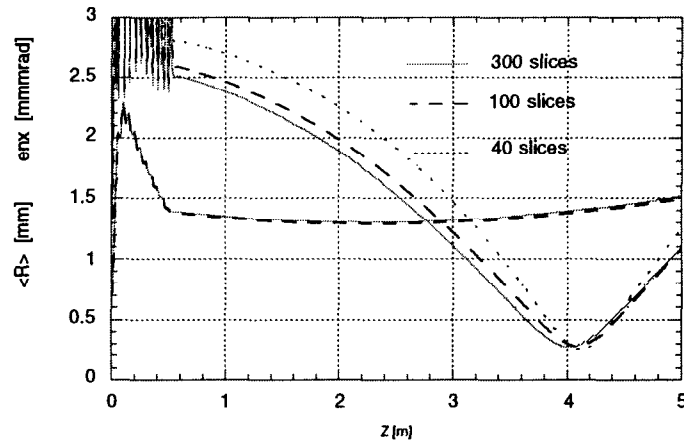


**Figure 8.** Envelope and emittance along the FABRE injector beamline as computed by HOMDYN with increasing number of slices.

In the lower part of the plot is shown the emittance of the core of the bunch, 10% of particles, as computed by ITACA, clearly showing by comparison the strong contribution of the head and tail of the bunch to the emittance value. We

investigated also the origin of the disagreement close to the cathode by increasing the number of slices per bunch from 40 to 300 in the HOMDYN simulations. In this case the solenoid strength has been slightly reduced corresponding to the best emittance performance of this device. The results, see Fig. 8, show a tendency to reduce the emittance value close to the cathode while leaving almost unchanged the absolute minimum.

We can conclude from these comparisons that HOMDYN is a reliable and fast tool to investigate a new injector configuration and the parameter space as long as non linear space charge effects are negligible. A final cross check with a multi-particle code is anyway mandatory.

## 5 The new working point for a split photoinjector

In Fig. 9 the accelerating and the solenoid fields as designed for the GTF gun are shown. It is interesting to note that the peak solenoid field is located downstream the gun cavity exit, at  $z=0.19$  m. The solenoid is designed to have no magnetic field at the cathode location, without any bucking coil.

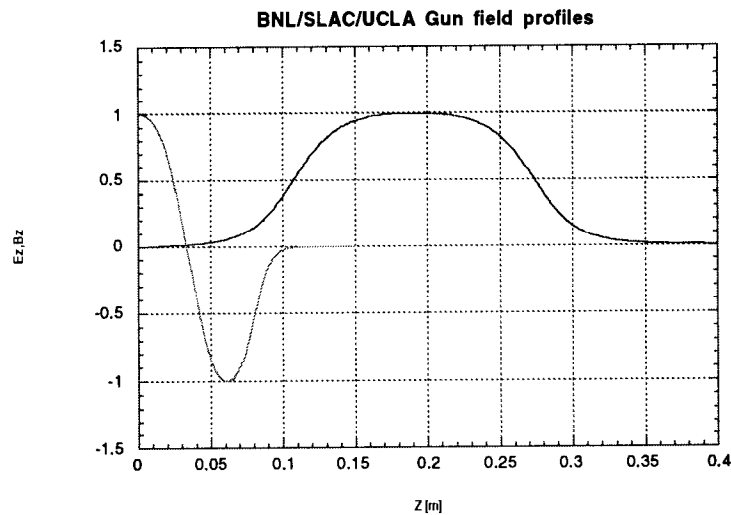


**Figure 9.** Accelerating and solenoid fields as designed for the GTF split photoinjector experiment.

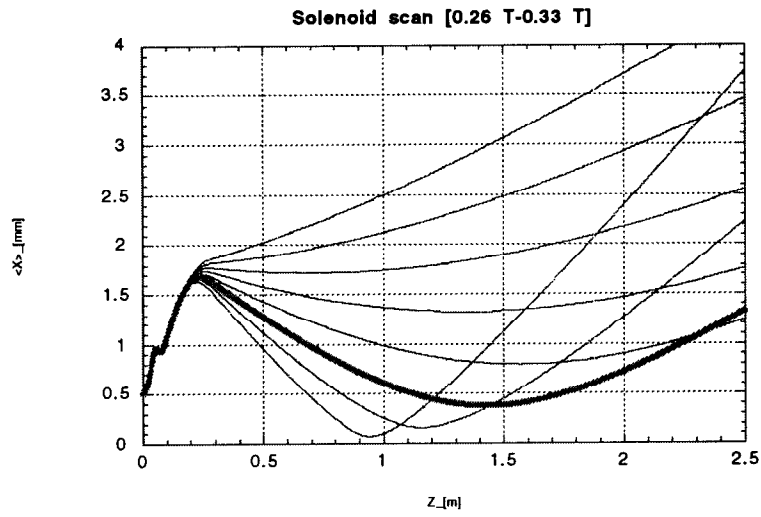


**Figure 10.** Beam envelope versus  $z$  for different solenoid strengths.

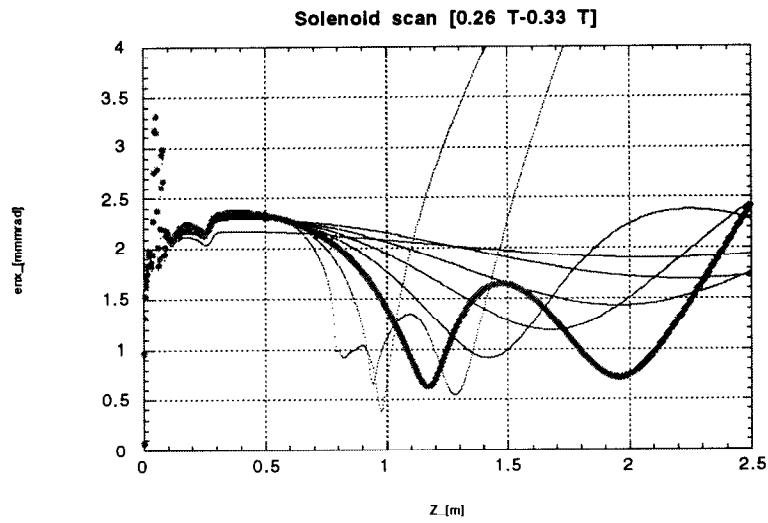


**Figure 11.** Beam emittance versus  $z$  for different solenoid strengths.

A detailed systematic PARMELA analysis of this gun and beam parameters can be found in [19]. Good emittance performances and high peak current at the exit of the device can be obtained with high peak field on the cathode (140 MV/m), extraction phase 35 deg and moderate solenoid field strength (0.3 T), for a 1 nC charge and 10 ps long bunch with 1 mm radius. In the following analysis we will take these parameters as a starting point.

We adopted the code HOMDYN to extend the investigation to the booster matching condition, taking advantage of the fast running capability of the code to explore a wider range of parameters. The booster matching condition indeed requires the beam to be injected at a laminar waist, as discussed in section 2. The booster location and accelerating gradient depend in a complicated way on many gun parameters, in particular, for a given bunch charge and dimension, they depend on the gun peak field, extraction phase and solenoid strength.

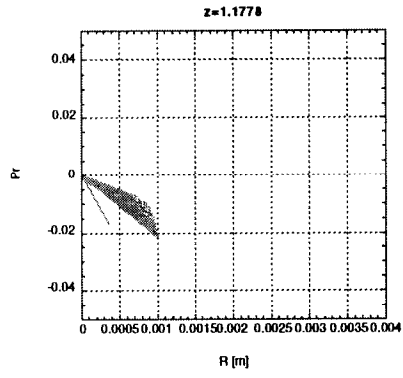
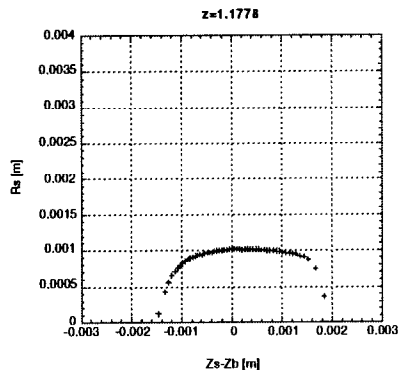
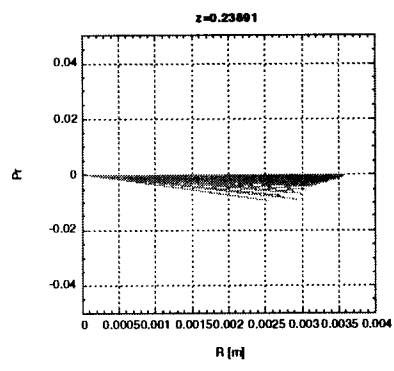
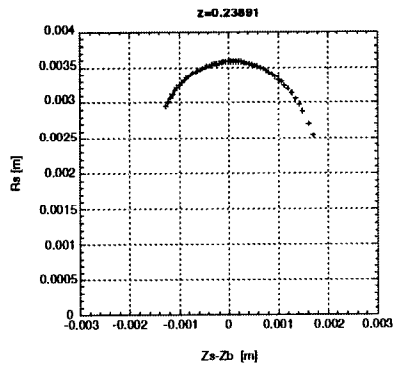
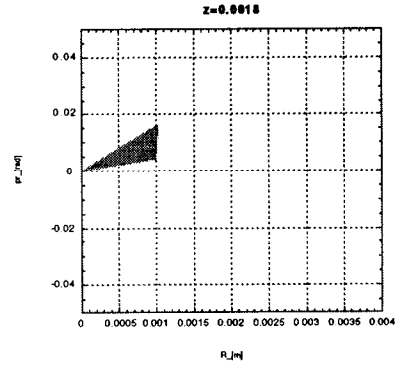
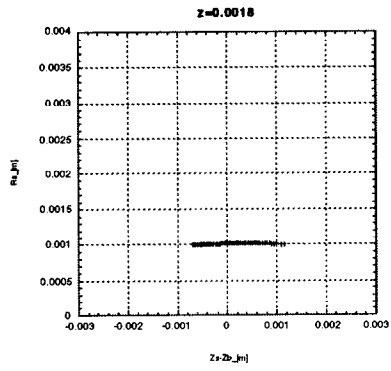
While investigating the envelope and emittance behaviour by scanning the solenoid field strength we noticed an interesting feature. By increasing the solenoid strength the emittance evolution shows a double minimum behaviour in the drifting region. For a given value of the solenoid strength (0.31 T) the envelope waist occurs ( $z = 1.5$  m) where the emittance has its relative maximum as shown by the bolded red lines in Figs. 10 and 11. The new working points performances rely on this feature of the emittance oscillation. The guess is that if we locate the booster entrance at  $z = 1.5$  and we satisfy the matching condition, the second emittance minimum could be shifted at higher energy and frozen at a lower level, taking profit of the additional emittance compensation occurring in the booster.

In Figs. 12 the longitudinal cross section of the bunch and the phase space are shown at five locations: at the very beginning after 10 ps ( $z = 0.0018$  m), at the envelope maximum ( $z = 0.23891$  m), at the first emittance minimum ( $z = 1.1778$  m), at the relative emittance maximum ( $z = 1.5$  m) and at the second emittance minimum ( $z = 1.9463$  m).

Each slice is represented in the phase space as a straight line, radial non linearities being neglected, connecting the axis origin with the slice envelope coordinates  $(R_s, \beta_s \gamma_s R_s')$ . As discussed in [20] the rms emittance is equivalent to the statistical mean area of all the triangles  $(O, R_s, \beta_s \gamma_s R_s')$ . In the first three couple of plot is clearly visible the initial bunch blow up and emittance compensation process downstream the solenoid location while the full bunch is convergent. The compensation reaches the first minimum when the head and the tail of the bunch are very close to an emittance dominated waist, then a trajectory cross over the axis may occur leading to an emittance increase.

When the main body of the bunch goes through the laminar waist (fourth couple of plots) the slices are all divergent and the corresponding triangles are more overlapped in the phase space, leading to the second emittance minimum (fifth couple of plots).





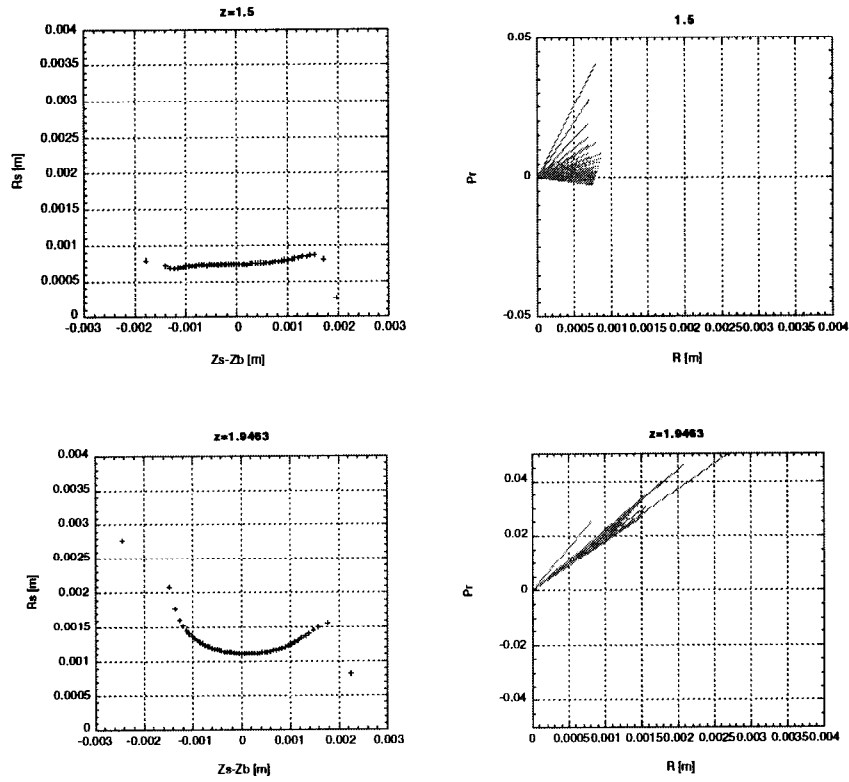


**Figure 12.** Longitudinal bunch cross section (left column) and transverse phase space (right column) at five different locations.: at the very beginning after 10 ps ( $z = 0.0018$  m) when the tail of the bunch is just extracted, at the envelope maximum ( $z = 0.23891$  m) right after the solenoid center, at the first emittance minimum ( $z = 1.1778$  m), at the relative emittance maximum ( $z = 1.5$  m) corresponding to the laminar waist position and at the second emittance minimum ( $z = 1.9463$  m).

It is interesting to note also in the longitudinal phase space the huge energy spread (3%) at the waist location and the corresponding current distribution within each slice, see Fig. 13. The question is now: *what happens when post acceleration is taken in to account?*

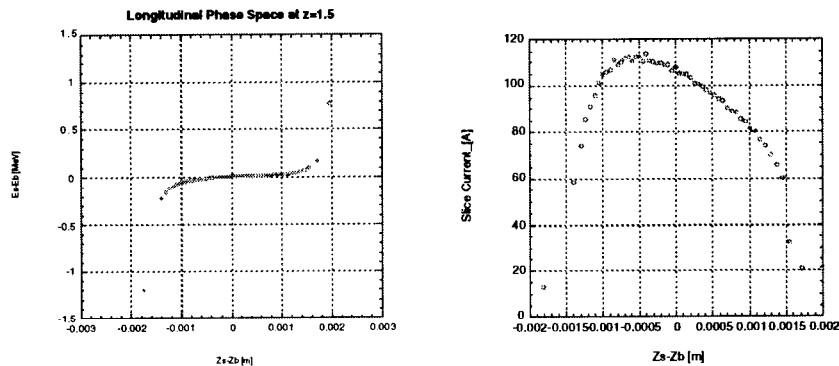


**Figure 13.** Longitudinal phase space and current distribution within each slice at the waist location  $z=1.5$  m.

## 6 The LCLS case

As a first natural choice for the booster linac we consider a 3 m long constant gradient S-band TW structure, in use at SLAC since the 1960s [21]. To satisfy the first matching condition, eq. (3), the booster should be located at  $z = 1.5$  m, where the beam laminar waist occurs. Since the rms spot size is  $\sigma_x = 0.41$  mm, the current averaged over the slices is 96 A and the average slice energy is 6.4 MeV, the matched accelerating gradient of the TW booster, eq. (5), is required to be 35 MV/m. To drive the beam out of the space charge dominated regime we need two SLAC structures resulting in an energy of 216 MeV in an 8 m long injector line, taking a 0.5 m long drift in between the two structures.

As expected the second emittance minimum, 0.5 mm-mrad, occurs now downstream the booster structures, see Fig. 14, at  $z = 10$  m (we will take this location as a reference position to quote emittance at the injector exit). An injection into the booster 12 degrees off crest is sufficient to compensate for the energy spread, resulting in a residual rms energy spread at the exit of the booster of 0.2 % , see Fig. 15, as required for the LCLS specifications. The peak current is 96 A slightly below the expected value. Bunch cross section and corresponding phase space are shown in Fig. 16 at the injector exit.

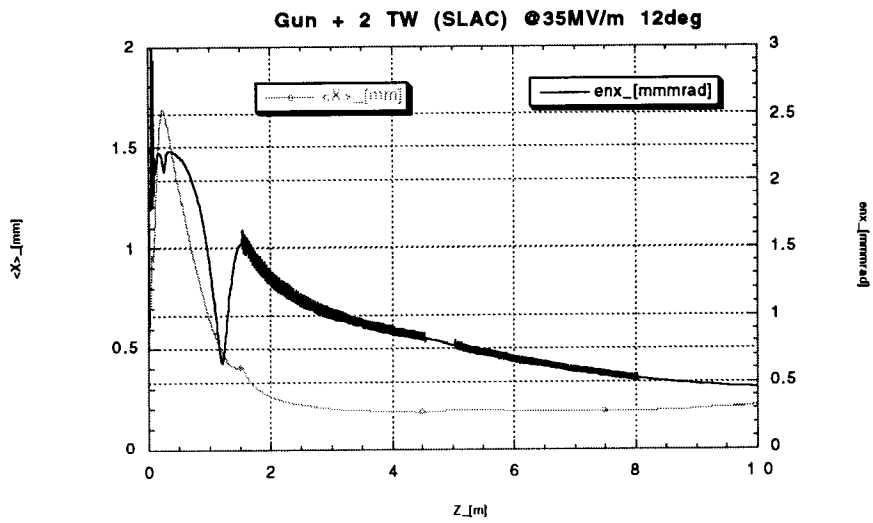


Figure 14. Beam envelope and emittance along the injector beam line.

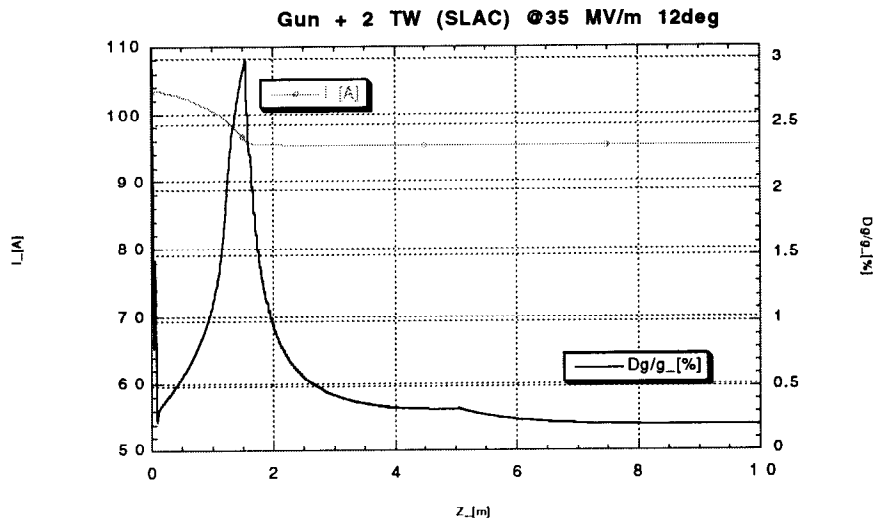


Figure 15 - Peak current and rms energy spread along the injector beam line.

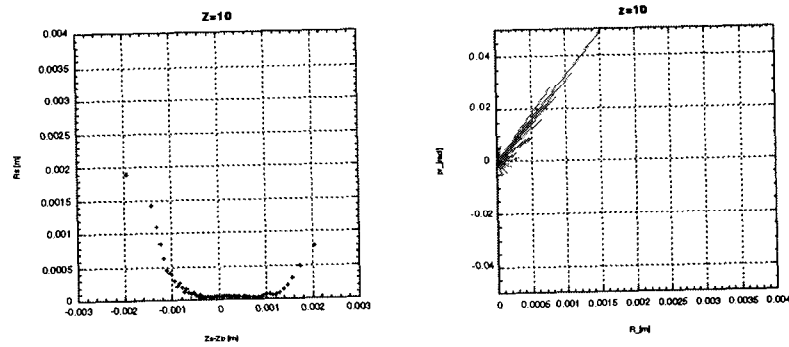


Figure 16 - Longitudinal bunch cross section (left) and transverse phase space (right) at the injector exit,  $z=10$  m.

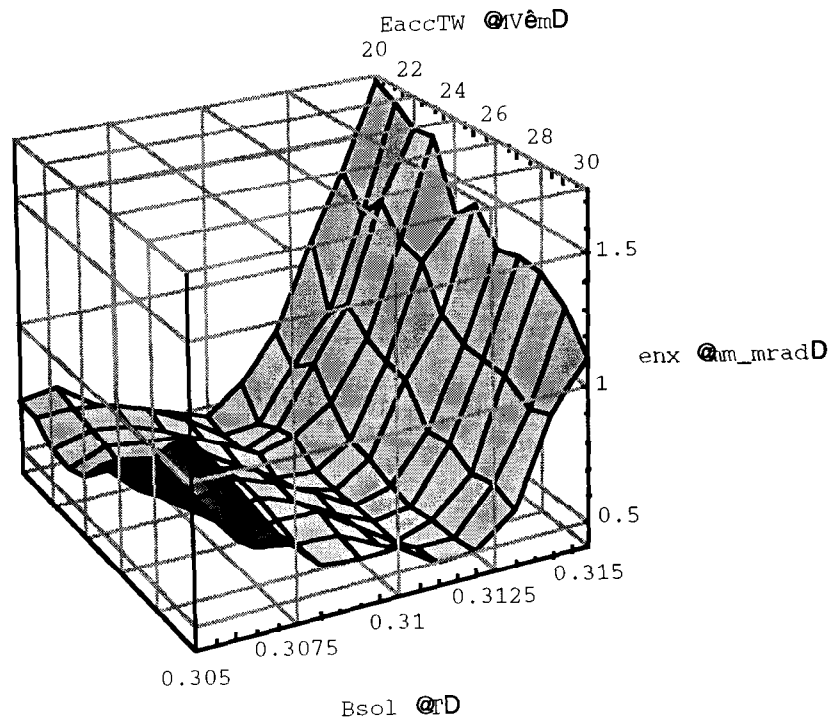


Figure 17. Cross scan of the gun solenoid strength and the booster accelerating field for TW sections.

Despite the good emittance resulting from this design, the necessary gradient to match the beam to the booster is exceeding the limit of a reliable performance of the SLAC structure. We then started to look for a lower gradient solution. The first attempt was of course to cross scan the gun solenoid strength and the booster accelerating field around a more reasonable value: 25 MV/m. An inspection of Fig. 17 shows a nice valley for the emittance minimum versus the accelerating field even if the width of the valley tends to become narrower as the accelerating field decreases.

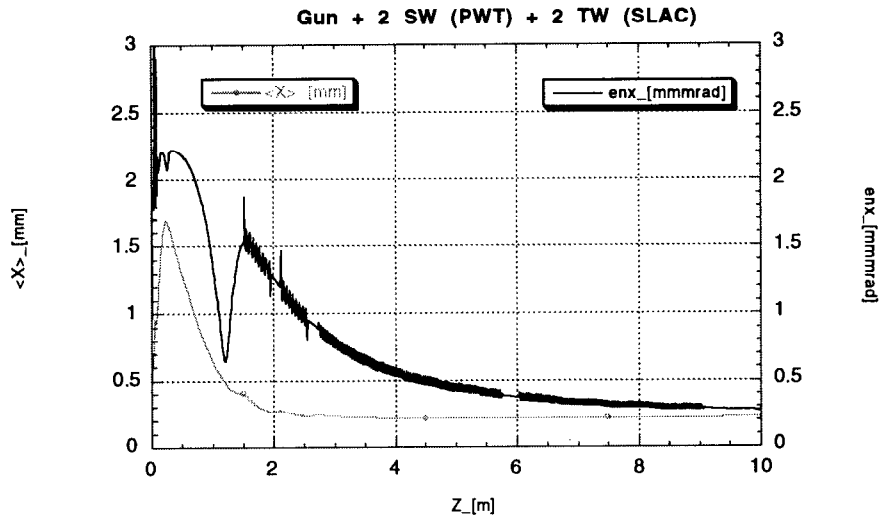


Figure 18. Beam envelope and emittance along the injector beam line.

Another possibility, as originally presented in [8], was to take advantages of the lower gradient necessary to match the beam to a SW booster linac. In the Neptune laboratory at UCLA for example, one 0.5 m long SW structure of the Plane Wave Transformer type (PWT) [22] is currently working at 25 MV/m. In our case the optimum accelerating field would be 28 MV/m, eq. (4), and to reach the required energy at least 11 PWT cavities would be necessary. In the following test we considered the possibility of reducing the number to two PWT cavities operating at 28 MV/m followed by two TW SLAC structures. As required from the invariant envelope theory the bunch at the exit of any well matched accelerating structure should have an envelope parallel to axis. Our matching also satisfy this requirement as shown in Fig. 18. We can now compute the accelerating field to match the beam to the 2 TW structures.

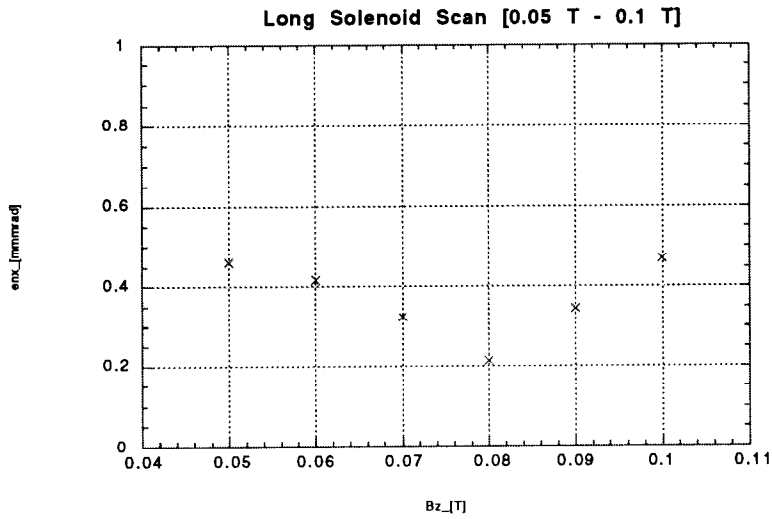


Figure 19. RMS normalised emittance at the injector exit, versus long solenoid scan.

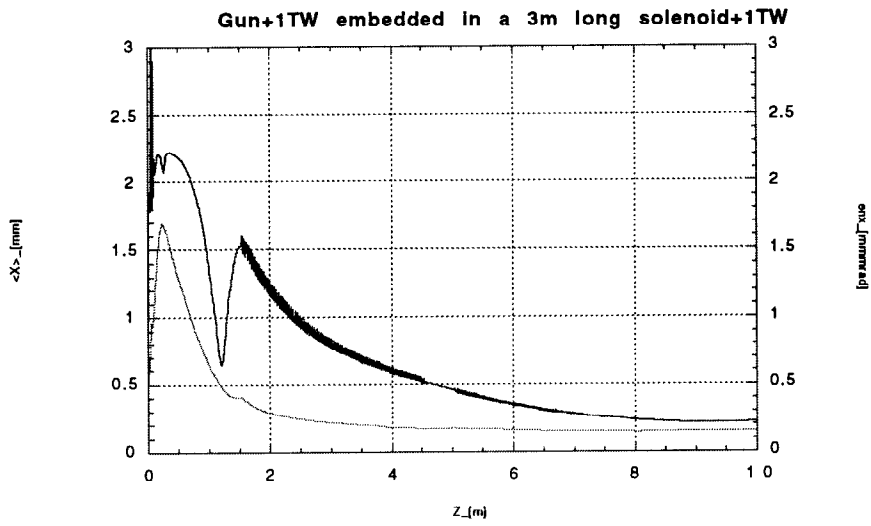


Figure 20. Beam envelope and emittance along the injector beam line.

A possible location of the first TW structure is at  $z = 2.7$  m, where the rms spot size is  $\sigma_x = 0.24$  mm, the current averaged over the slices 95 A and the average slice energy 33.4 MeV. The matched accelerating gradient of the TW booster is required to be 26.6 MV/m. This result is very promising giving an output emittance down to 0.27 mm-mrad. In addition the length of the full injector by this design is approximately within the limit of the available room.

We then decided to increase the focusing properties of the device without using the SW structures. This can be done by means of a long solenoid around the first TW structure, now located back at  $z = 1.5$  m. The equivalent solenoid strength of the backward component in a SW structure is given by:  $B = \frac{E}{\sqrt{2}c} = 660$  G for a 28

MV/m accelerating field. Setting the desired accelerating field of the TW section to 25 MV/m a scanning of the solenoid strength around the computed value showed a very good working point with  $B = 800$  G as shown in Fig. 19. The simulation showed an incredibly low emittance value 0.2 mm mrad, see also Fig. 20, fulfilling at the same time the other LCLS requirements.

## 7 PARMELA computations

To inspect the contribution of the non-linear radial space charge field on the beam dynamics, we cross checked HOMDYN results with the code PARMELA. This version of PARMELA allows particle loading by Quiet Start and a high resolution mesh size as required to properly simulate a perfect cylindrical uniform beam. To limit CPU time we considered initially the Neptune like configuration using the gun plus 2 SW PWT cavities only, without additional acceleration. The beam line considered in the following simulation is slightly different from the one described in the previous section, in particular the solenoid field considered is the one of the Neptune injector. Nevertheless the new working point requirements are fulfilled and the results confirm also the stability of this design.

The pulse is uniform over ten picoseconds, has a radius of 1 mm and vanishes outside of these boundaries. The total charge injected is 1 nC, and the peak accelerating fields in the rf gun and PWTs are 140 MV/m and 58 MV/m, respectively. The focusing solenoid is adjusted to produce a matched invariant envelope in the PWT post-acceleration sections, that in this case occurs at  $z = 1.6$  m. Fig. 21 shows the extremely good rms normalised emittance achieved (0.4 mm-mrad) in this design after a final drift to roughly 4 m from the cathode. It should be noted that the size of the beam on the cathode, and its size at the first compensation point (end of first beam size oscillation) are nearly identical in this optimised design.



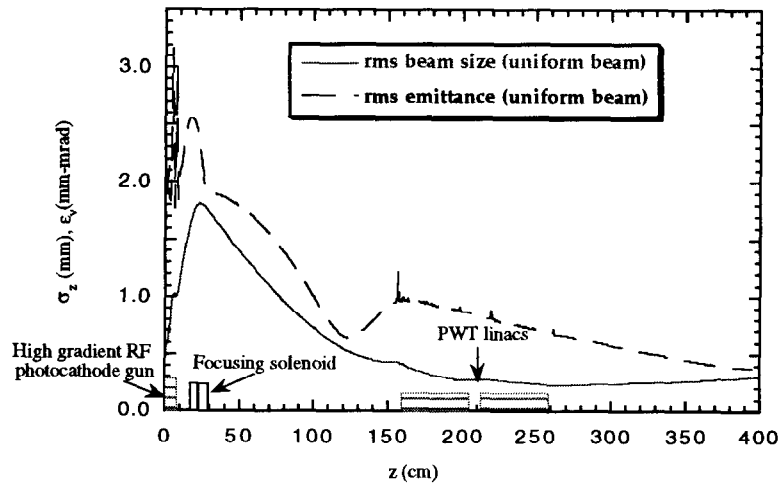


**Figure 21.** Results of PARMELA simulation of uniform beam emitted at cathode in LCLS photoinjector design, with 1.6 cell rf gun followed by an emittance-compensating solenoid, and two PWT standing wave sections.

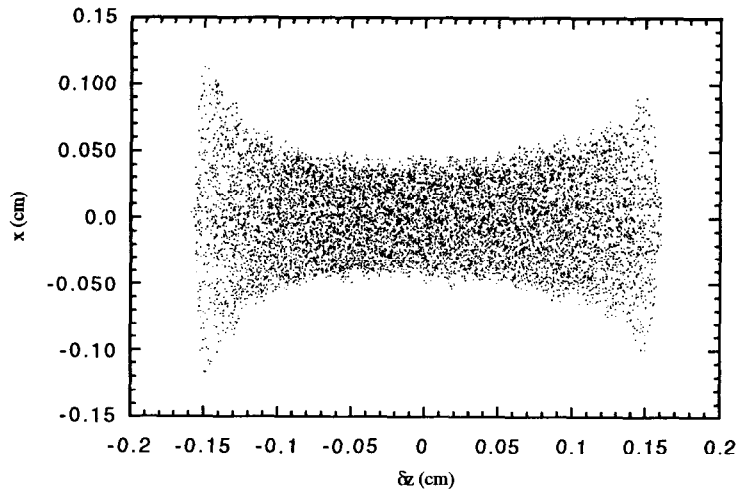


**Figure 22.** Bunch cross section at the end of PARMELA simulation shown in Fig. 21.

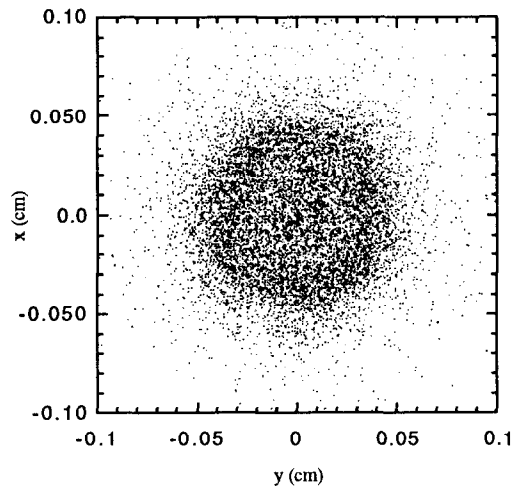


**Figure 23 (a).** Spatial  $(x,y)$  distribution at the end of PARMELA simulation shown in figure 21.

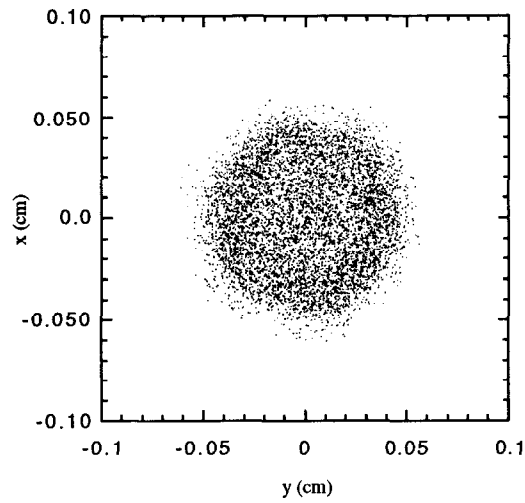


**Figure 23 (b).** Spatial  $(x,y)$  distribution at the end of PARMELA simulation shown in figure 21, with cut made on the distribution at  $\delta z = \pm 0.1$  mm, to remove longitudinal tails.

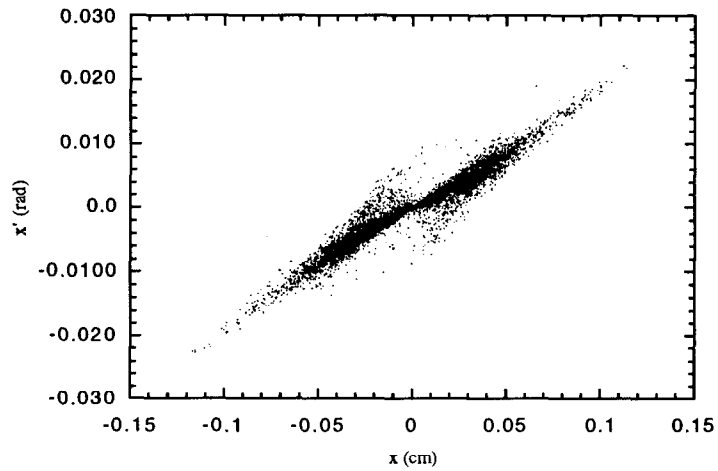


**Figure 24 (a).** Phase space distribution at the end of PARMELA simulation shown in figure 21.

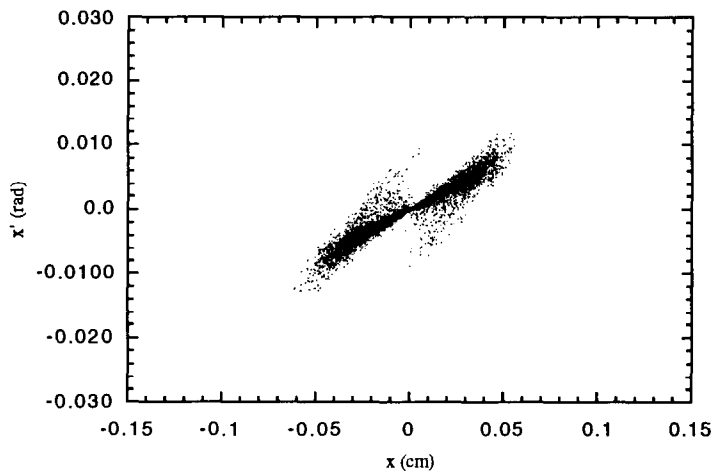


**Figure 24 (b).** Phase space distribution at the end of PARMELA simulation shown in figure 21, with cut made on the distribution at  $\delta z = \pm 0.1$  mm, to remove longitudinal tails.

This fact points to the close relationship that interslice (linear) and intraslice (nonlinear) emittance oscillations have with each other, as discussed in [23]. The  $(x,z)$  spatial profile of the 10,000 simulation particles at the  $z=4$  m point is shown in Fig. 22. It can be seen that, while the core of the beam is well behaved in terms of the different  $z$ -slices, ending up in the same configuration, the leading and trailing beam edges display very different behaviours. This is due to the fact that the transverse space-charge forces drop dramatically in these longitudinal “tail” regions, and the particles in these slices do not focus to space-charge dominated waists, but in fact cross the beam axis, as observed also in [24] for a different case. This is clearly nonlaminar flow, and as a result, the total transverse phase space bifurcates into two populations. One population is composed of slices which have essentially no wave-breaking associated with them, and another in which beam particles wave-break near the origin. These populations can also be observed in the  $(x,y)$  spatial distribution shown in Fig. 23(a), and the phase space distribution displayed in Fig. 24(a). In Fig. 23(a), the bifurcated population, i. e., the population that experience axis cross over, produces a slight beam halo, while in Fig. 24(a), one can directly see the bifurcation as distinct lengths of the slices in phase space.

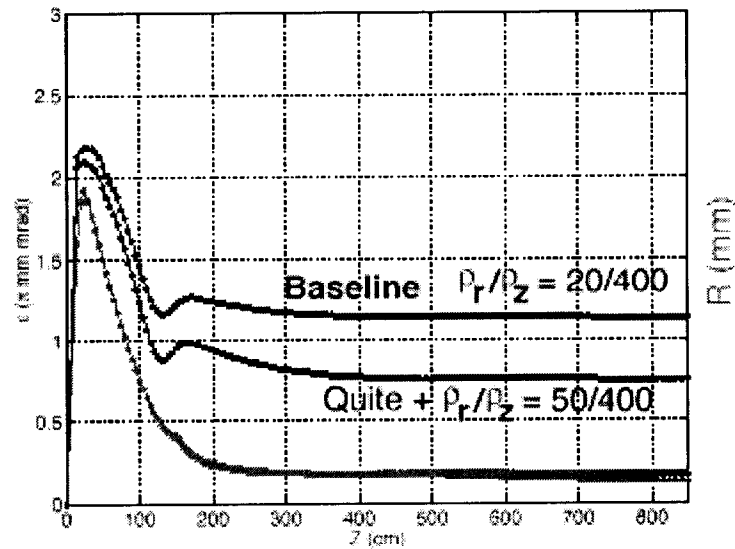


**Figure 25.** Envelope (red line) and Emittance (blue lines) along the beam line computed with two different space charge mesh size

These points are emphasised by Figs. 23(b) and 24(b), in which the  $(x,y)$  spatial and phase space distributions are shown for the beam population located only within  $\delta z = \pm 0.1$  mm from the beam longitudinal center. In Fig. 23(b), the beam halo essentially disappears when this cut is made. In Fig. 24(b), one sees a very interesting situation — even though the longitudinal tails have gone

bifurcated, they are *realigned in phase space* with the beam cores. The difference between the bifurcated and unbifurcated populations is simply that the length in phase space is larger for the bifurcated population in the longitudinal tails.

We report in conclusion a very interesting PARMELA result concerning the first solution considered for the LCLS: the gun followed by two TW SLAC structures. With a standard mesh point number of 20x400, (i.e, the space charge field is computed over a matrix composed by 20 radial rows and 400 longitudinal columns) the cross check with HOMDYN results, see Fig. 14, was quite discouraging. As shown in Fig. 25, the computed emittance never went below 1 mm-mrad. However, by increasing the mesh points from 20x400 to 50x400, the agreement is much better, with a rms normalised emittance predicted by PARMELA of 0.8 mmmrad. A more systematic comparison between HOMDYN and PARMELA computations can be found in [25].

## 8 Conclusions

By investigating a new design for the LCLS injector, a new stable working point for a split photoinjector has been found.

Three different injector options have been analysed:

1. Gun + Drift + 2 TW SLAC structures
2. Gun + Drift + 2 SW PWT structures + 2 TW SLAC structures
3. Gun + Drift + 2 TW SLAC structures the first one embedded a Long Solenoid.

Option # 3 fully satisfies the LCLS requirements with reasonable accelerating fields.

A more detailed analysis has to be done with a more realistic beam, i. e., taking in to account Gaussian tails. Nevertheless the results of section 7 allow one to think that the contribution of the tails can be kept under control. At the same time an experimental program is under way at the SLAC GTF facility, in order to measure the double emittance feature along the beam line [26] and to determine experimentally the proper location for the booster linac.

## 9 Acknowledgements

Many helpful discussions with J.F. Schmerge (SSRL), M. E. Hernandez (Stanford), D. Nguyen (LANL) and D. H. Dowell (Boeing), all members of the GTF team at SLAC during the summer of 1999 when the bulk of this paper was being produced, are gratefully acknowledged. One of us (M. F.) wishes to thank the SLAC staff for the kind hospitality during his stay at SLAC in that same period.

## References

1. J.F. Schmerge et al., "Photocathode rf gun emittance measurements using variable length laser pulses," *SPIE* 3614 (1999) 22.
2. L. Serafini and J.B. Rosenzweig, "Envelope analysis of intense relativistic quasilaminar beams in rf photoinjectors: A theory of emittance compensation," *Phys. Rev. E* 55 (1997) 7565.
3. D.T. Palmer et al., "Emittance studies of the BNL/SLAC/UCLA 1.6 cell photocathode rf gun," *Proc. of the 1997 Particle Accelerator Conf.* (1997) 2687.
4. M. Babzien et al., "Observation of self-amplified spontaneous emission in the near-infrared and visible," *Phys. Rev. E* 57 (1998) 6093.
5. J. Clendenin et al., "Reduction of thermal emittance of rf guns," to be published in the *Proc. of the Int. Sym. on New Visions in Laser-Beam Interactions, Tokyo, Oct. 11-15, 1999* see also SLAC-PUB-8284 (1999)
6. R. Alley et al., "The design for the LCLS rf photo-injector", *Nucl. Instr. and Meth. A*, 429 (1999), 324-331.
7. D. T. Palmer et al., "Simulations of the BNL/SLAC/UCLA 1.6 Cell Emittance Compensated Photocathode RF Gun Low Energy Beam Line", *Proc. of the 1995 Particle Accelerator Conf.* (1995), p. 2432.
8. B. Carlsten and M. Ferrario, "Photoinjectors", *Proc. of the ICFA Workshop on Future Light Sources, Argonne, April 99*, now available on the web: <http://www.aps.anl.gov/conferences/FLSworkshop/>
9. M. Ferrario et al., "Multi-bunch energy spread induced by beam loading in a standing wave structure", *Particle Accelerators*, 1996, Vol. 52 (1).
10. K. Halbach and R. F. Holsinger, "SUPERFISH - a computer program for evaluation of RF cavities with cylindrical symmetry", *Particle Accelerators*, 1976, Vol. 7 (213).
11. J. Sekutowicz, M. Ferrario, Ch. Tang, "Superconducting Superstructure for the TESLA collider, a concept" *Phys. Rev. ST-AB*, V. 2, 062001, June 1999
12. J. Haimson, "Electron bunching in traveling wave linear accelerators", *Nucl. Instr. and Meth.* 39 (1966) pp 13-34.
13. J. Rosenzweig and L. Serafini, "Transverse particle motion in radio-frequency linear accelerators", *Phys. Rev. E* 49 (1994) 1599.
14. G. A. Loew et al., "Computer calculations of traveling-wave periodic structure properties" SLAC-PUB-2295, March 1979
15. L. Serafini and C. Pagani, "ITACA: a new computer code for the integration of transient particle and field equations in axi-symmetrical cavities", *Proc. of I EPAC, Rome, 1988, World Sci., Singapore*, p.866.
16. L. Serafini, *these proceedings*
17. Rossbach et al., "A VUV Free Electron Laser at the TESLA Test Facility at DESY, Conceptual Design Report", *TESLA-FEL note 95-03*
18. L. Serafini et al., "The FABRE project: design and construction of a integrated photo-injector for bright electron beam production", to be published on *Proc. Of EPAC 2000, Vien.*

19. D. T. Palmer, "The next generation photoinjector", *PhD. Thesis, Stanford University*.
20. J. Buon, "Beam phase space and emittance", *Proc. Of CAS, Univ. of Jyvaskyla, Finland, September 1992, CERN 94-01*.
21. R. B. Neal et al., "The Stanford two-mile accelerator" *W. A. Benjamin, Inc., New York-Amsterdam (1968)*.
22. S. Anderson et al., "Commissioning of the NEPTUNE photoinjector", *Proc. Of PAC99, New York, p. 2006*.
23. J. B. Rosenzweig and S. Anderson, *these proceedings*.
24. L. Serafini, "Overview on Production and Dynamics of High Brightness Beams", *AIP CP 395, 1997, p.47*.
25. M. Ferrario and D. T. Palmer, "HOMDYN/PARMELA comparison about a high gradient solution for the LCLS photoinjector", *to be published*.
26. M. Ferrario et al., "A new low-emittance, high gradient design for the LCLS photoinjector", *to be submitted to Phys. Rev. ST-AB*